# Defect Structure of Nonstoichiometric $CeO_2(111)$ Surfaces Studied by Scanning Tunneling Microscopy

H. Nörenberg* and G. A. D. Briggs

*University of Oxford, Department of Materials, Parks Road, Oxford OX1 3PH, United Kingdom*

(Received 23 July 1997)

The surface structure of nonstoichiometric $CeO_2(111)$ has been studied by scanning tunneling microscopy (STM). By using extremely small tunneling currents it was possible to obtain the first ever reported atomically resolved images of this oxide. STM imaging was possible at a sample bias voltage between $-2$ and $-3.5$ V. Comparing this with the band structure of ceria we claim that the main contribution to the image contrast results from oxygen in the topmost layer. The dominant defect type on the surface at RT is of triangular shape and contains three oxygen vacancies. Elevated temperature STM at a substrate temperature of 500 °C revealed an alignment of oxygen vacancies on the surface. The defect shapes are in qualitative agreement with previous energy calculations. [S0031-9007(97)04549-3]

PACS numbers: 68.35.Bs, 61.16.Ch, 68.35.Dv

$CeO_2$ is an electrically insulating oxide which crystallizes in the fluorite structure. It has a band gap of 3.2–6 eV [1–4] and becomes conductive after creating oxygen vacancies. Oxygen vacancies can either be created in the bulk by annealing [5] with subsequent diffusion to the surface, or they can be created directly at the surface by annealing, sputtering [3], electron irradiation [6], exposure to x rays [7], or chemical reduction [8]. The surface defect structure of $CeO_2$ is believed to play a key role in catalytic reactions [9]. From x-ray photoelectron spectroscopy (XPS) [10], electron paramagnetic resonance (EPR), and Fourier transform infrared (FTIR) spectroscopy [11], there is strong experimental evidence that upon reduction $Ce^{4+}$ is transformed into $Ce^{3+}$ both in the bulk and at the surface. The defect structure of $CeO_2$ has previously been studied by XPS and high resolution electron energy-loss spectroscopy (HREELS) [3], diffuse reflectance spectroscopy [8], FTIR [8,11], EPR [11], resonant photoemission [12], and surface energy calculations [13,14]. Based on these studies the existence of oxygen vacancies on the ceria surface was postulated, but no experimental characterization of their arrangement has been carried out so far. Calculations showed that vacancies are more stable at the surface than in the bulk [13,14] and that certain arrangements of pairs of vacancies lower the total energy of the (111) surface [13]. The association of vacancy centers was concluded from EPR experiments [11]. Most of the experimental investigations cited above were carried out on polycrystalline samples or thin films which complicates the interpretation of the results because different crystallographic surfaces are supposed to show different defect structures [13,14]. A direct observation of the size and shape of oxygen vacancies, however, is not available so far. The present study aims to contribute to the understanding of the structure of the $CeO_{2-x}(111)$ surface by using the real space capability of a scanning tunneling microscope (STM) to image the surface structure on the atomic scale.

Epipolished $CeO_2(111)$ wafers supplied by Commercial Crystal Laboratories Inc. were used as substrates. Impurities were below the detection limit of energy-dispersive x-ray (EDX) spectroscopy. The greyish appearance of the crystals was probably caused by traces of CaO which might also be responsible for the conductivity of $1 \times 10^{-3}$ $(\Omega\ \mathrm{cm})^{-1}$ [15]. To further increase the conductivity of the samples they were annealed at 1000 °C for a few minutes under UHV conditions. The conductivity of the reduced sample under UHV conditions was approximately 0.1 $(\Omega\ \mathrm{cm})^{-1}$ at 1000 °C and 0.02 $(\Omega\ \mathrm{cm})^{-1}$ at room temperature (RT). Based on previous conductivity measurements at RT and elevated temperatures [5,16], we estimated the degree of nonstoichiometry of our $CeO_{2-x}$ sample as $x = 0.01 \pm 0.005$ and therefore refer to our sample as $CeO_{1.99}$. Nonstoichiometric ceria maintains its fluorite structure as $CeO_{2-x}$ with $(0.15 < x < 0.0005)$ [17].

The RT STM experiments were carried out with an OMICRON STM1 working at a base pressure of $3 \times 10^{-11}$ mbar under RT conditions. Although the samples still had a conductivity of only 0.02 $(\Omega\ \mathrm{cm})^{-1}$, it was possible to obtain STM images at RT at very low tunneling currents in the range 10 to 20 pA. By choosing a sample holder with a specially designed geometry it was possible to reduce the resistance between the area under observation and the grounded sample holder sufficiently. Another way of overcoming the poor conductivity is imaging at higher temperatures as the conductivity of ceria increases with temperature. Experiments at elevated temperatures were carried out with a JEOL JSTM 4500-XT in the range up to 500 °C. Lateral distance and height measurements were calibrated against a Si(001) standard. Commercially produced, etched Pt-Ir tips were used. The chemical composition of the surface during preparation was monitored by Auger electron spectroscopy (AES) with a primary electron beam energy of 3 keV. Reflection high energy

 0031-9007/97/79(21)/4222(4)$10.00 

electron diffraction (RHEED) and low energy electron diffraction (LEED) were used to monitor the surface morphology *in situ* during surface preparation.

Figure 1 shows a large scale STM image of the $CeO_{1.99}(111)$ surface taken at RT. There are large regions where the surface appears well ordered and atomically flat (O), and regions with predominantly triangular surface defects (D). The inset in Fig. 1 shows a height profile across a step edge as indicated in Fig. 1. Adjacent terraces are separated by a single step height of $2.9 \pm 0.4$ Å which compares favorably with the accepted value of 3.13 Å. The $(1 \times 1)$ termination of the surface was confirmed by LEED and RHEED. It agrees with the fact that no significant lateral relaxation was found in calculations of $CeO_2(111)$ [13]. The AES spectrum in Fig. 2 shows a clean ceria surface with traces of impurities which can be identified as carbon and calcium. Carbon most likely comes from vacuum contamination, whereas calcium is a known addition in $CeO_2$ [15]. The small peak at 185 eV originates from the Mo sample holder.

Figure 3 shows a close-up of the well ordered $(1 \times 1)$ surface structure shown in Fig. 1. The well ordered regions show the $(1 \times 1)$ bulk termination with an interatomic distance of $(4.0 \pm 0.2)$ Å which is very close to the crystallographic value of 3.82 Å. It is generally agreed upon that the topmost layer of (111) oriented fluoritelike oxides consists of oxygen [18] to avoid a polar surface. The argument that oxygen forms the topmost layer is further supported by surface defect studies which showed that there are oxygen vacancies on ceria surfaces [3,8,11]. In our experiments atomic resolution could be obtained by imaging filled states in the bias voltage range $-2$ to $-3.5$ V. The main feature of the bulk band structure of $CeO_2$ is a broad band of oxygen $2p^6$ states with $4f$ and $5d$ character which stretches between $-1.8$ and $-4.5$ V below the Fermi energy [1]. There is, however, some controversy in the literature about the exact occupation of the $4f^1$ states. Above $E_F$ there are only two strongly localized $4f^1$ states which are assumed to be completely empty in stoichiometric $CeO_2$ [6]. Other results suggest that up to 0.5 electrons are in the $4f$ states [12]. Comparing the bias voltage range where we were able to obtain atomically resolved images to the band structure [1], we conclude that the main contribution to the STM image contrast (Figs. 1 and 3) originates from the oxygen $2p$ states (this argument is independent of the occupation of the Ce $4f$ states). This claim is further supported by the characteristic defect structure visible after a short anneal to 1000 °C. Among different types of defects visible on the surface at RT (Fig. 1) the triangular type is dominant. Figure 4 shows two such defects at a higher magnification. These triangular defects occupy a few percent of the entire surface area. The atoms on the defect edge closest to the vacancies appear brighter by 0.3 Å compared to the flat areas on the surface. This height difference cannot be explained in terms of geometry alone (the Ce-O bond length differs by less than 0.1 Å between $CeO_2$ and $Ce_2O_3$) and must therefore be influenced by electronic effects. For the explanation of the enhanced brightness of oxygen ions at the defect edges (Fig. 4) one has to consider the possibility of a small charge transfer from the vacancies to these oxygen ions. This means that not all charge is transferred to Ce ions. This would be in agreement with the mixed valence concept [12,19]. In general, the vacancy formation on a (111) surface is energetically favorable compared to the bulk [10,13,14]. The creation of a triangular defect consisting of 3 oxygen vacancies can be written in

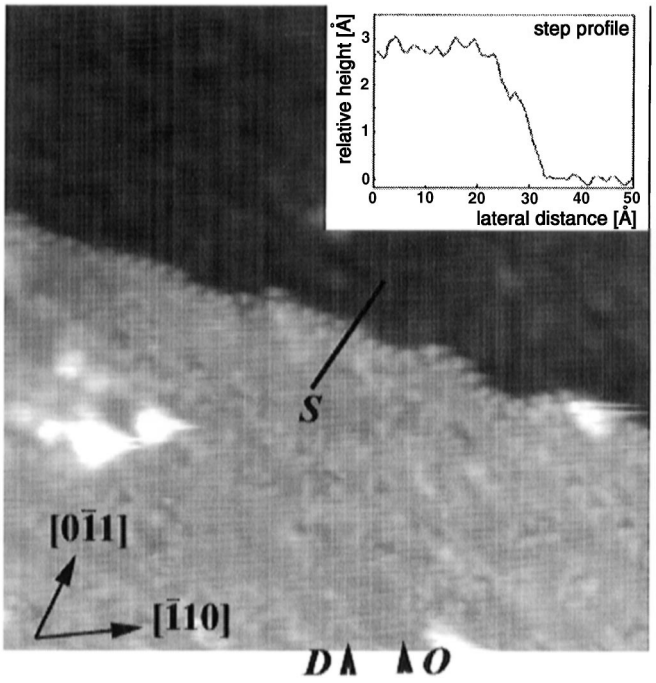


FIG. 1. STM image of nonstoichiometric $CeO_2(111)$ showing terraces separated by single step heights (see inset), image size 250 Å × 250 Å, $U_{\text{bias}} = -2.5$ V, $I_T = 15$ pA, RT; the inset shows a height profile across the line labeled *S*, *D* denotes a triangular defect, and *O* denotes an ordered region.

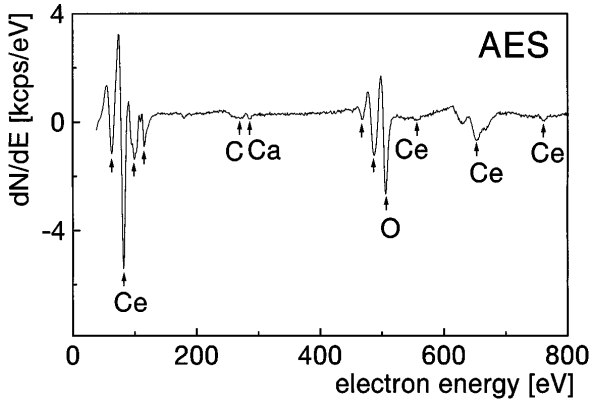


FIG. 2. Auger electron spectrum of nonstoichiometric $CeO_2(111)$, $E_p = 3$ keV.

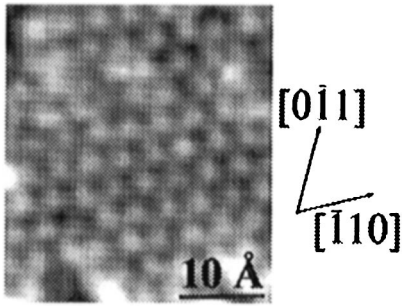


FIG. 3. Atomically resolved STM image of nonstoichiometric $CeO_2(111)$, image size 30 Å × 35 Å, $U_{bias} = -2.5$ V, $I_T =$ 10 pA, RT.

Kroger-Vink notation as

$$6\,Ce^{*}_{Ce} + 3O^{*}_{O} \longleftrightarrow 6\,Ce'_{Ce} + 3V_{\ddot{O}} + \tfrac{3}{2}O_2(g)\,.$$

In the light of these circumstances we propose the triangular defects to consist of three oxygen vacancies.

After keeping the sample at 500 °C for one day and taking STM images at 500 °C we observe a different defect structure. Figure 5 shows line defects dominating the STM image which were not visible up to 400 °C. They run along the $[01\bar{1}]$, $[10\bar{1}]$, and $[1\bar{1}0]$ directions. It appears that some of the line defects are originating from triangular defects, which are still visible at other locations.

Experimental evidence [8,20] suggests that oxygen is lost from the surface upon heating to 200–600 °C under reducing conditions or to above 600 °C under nonreducing conditions. Given the error margins of the temperature estimation and the duration of our annealing, the line defects may well be created by oxygen loss from the surface. The line defects (Fig. 5) exhibit an enhanced edge contrast similar to the triangular defects (Figs. 1 and 4). This helps to avoid low valent cations such as $Ca^{2+}$ from the defect structure.

Another possible explanation for the triangular defect is the presence of three low valent cations such as $Ca^{2+}$ on $Ce^{4+}$ sites and three oxygen vacancies. For our experiments we can exclude this possibility since the line defects visible at elevated temperatures (Fig. 5) show a similar contrast (enhanced brightness of the atoms adjacent to the missing oxygen positions). As two lines of Ce ions along $[2\bar{1}\bar{1}]$ run at different distances from the defect line, one would expect a different contrast on either side of a defect line which is not observed (Fig. 5). The brighter atoms on the defect edge themselves cannot be attributed to impurities as is evident from the low levels of impurities shown in the AES measurements (Fig. 2).

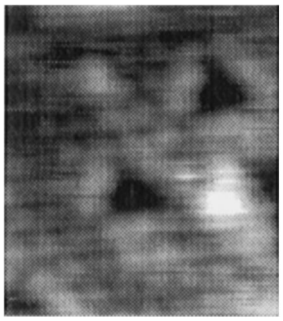

FIG. 4. STM image of triangular defects on nonstoichiometric $CeO_2(111)$ showing enhanced brightness at the defect edges, image size 35 Å × 40 Å, $U_{bias} = -2.5$ V, $I_T = 10$ pA, RT, same crystallographic orientation as Fig. 3.

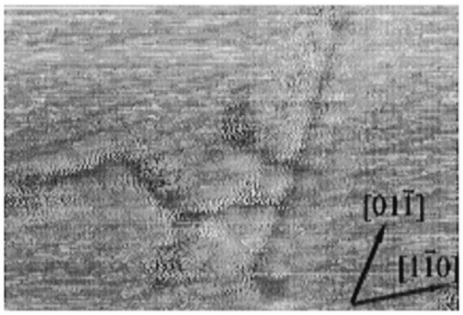


FIG. 5. Elevated temperature STM image of nonstoichiometric $CeO_2(111)$, image size 70 Å × 50 Å, $U_{bias} = -2.5$ V, $I_T = 1$ nA, $T = 500$ °C, same crystallographic orientation as Fig. 3.

Figure 6 shows a model of the (1 × 1) terminated (111) surface with its characteristic defects. In the upper left corner of Fig. 6 a triangular defect as observed by RT STM (Figs. 1 and 4) is shown. A defect consisting of two oxygen vacancies which was used in theoretical calculation [13] actually has the structure of a fragment of a triangular defect as indicated in the upper left part of Fig. 6. This defect shape gave the highest energy gain among all considered defect dimer configurations when formed from two separated oxygen vacancies (0.58 eV per vacancy pair) [13]. If this defect is filled with a

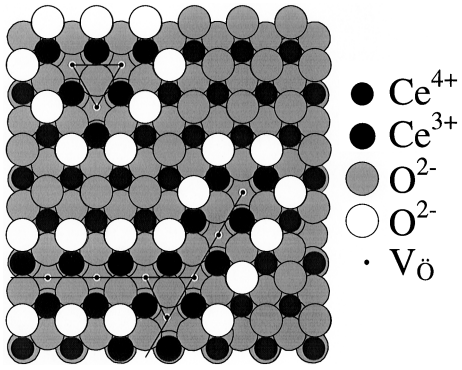


FIG. 6. Model of nonstoichiometric $CeO_2(111)$ showing the (1 × 1) terminated surface with triangular defects (upper left corner) and line defects (lower right corner); the edge oxygen ions are shown in a lighter shade; for details of the energy calculations of these defect structure see [13].

third vacancy to form a triangle a further substantial gain in energy is expected. Furthermore, the triangular shape reproduces the crystal symmetry and minimizes the $Ce^{3+}/V_{\ddot{O}}$ ratio as a function of the triangle size without creating $Ce^{2+}$ species (which have not been observed experimentally) on the surface. This is, of course, a simplified picture, but it might explain why there are a lot of triangular defects on the surface at RT consisting of three oxygen vacancies rather than point defects or vacancy pairs as previously suggested [8,13,14].

The lower part of Fig. 6 shows a typical line defect with a branch similar to the experimental observations (Fig. 5). Calculations suggest a small energy gain (0.19 eV per vacancy pair) if two initially separated oxygen vacancies form a linelike structure [13]. A triangular defect is visible where the two line defects meet (Fig. 6).

Because of the symmetry of the (111) fluorite structure a triangular structure of three anion vacancies can be arranged in two different ways: with a cation from the second layer in its center or with an anion from the third layer in its center. Both structures are indistinguishable by STM. However, it is highly unlikely to find Ce is in the center of the oxygen vacancy arrangement as it would leave the cerium in an apparent $Ce^{2+}$ state which is unfavorable.

In conclusion, we have shown that it is possible to obtain information about the atomic structure of slightly nonstoichiometric $CeO_2(111)$ surfaces by STM. The STM images taken at relatively high negative bias voltages probe states which are mainly derived from oxygen $2p$ states, and they show the topmost oxygen layer in an unreconstructed bulk terminated $(1 \times 1)$ structure. Surface defects consisting of oxygen vacancies have predominantly a triangular shape at RT; line defects can be observed at 500 °C. An oxygen vacancy of the defects observed on the (111) surface is in qualitative agreement with previous calculations of defect structures [13,14], but the STM images show in extension of these calculations that the defects generally consist of three rather than two oxygen vacancies.

The authors wish to thank J. H. Harding and C. Muggelberg for helpful remarks and S. L. Dudarev for fruitful discussion about charge transfer. We acknowledge the HCM fellowship ERBCHBICT961170 (H. N.). The work was supported by the EPSRC Grant No. GR/K08161.

*Corresponding author.
Electronic address:
holger.norenberg@materials.oxford.ac.uk

[1] F. Marabelli and P. Wachter, Phys. Rev. B **36**, 1238 (1987).
[2] S. M. Butorin *et al.*, Phys. Rev. Lett. **77**, 574 (1996).
[3] A. Pfau and K. D. Schierbaum, Surf. Sci. **321**, 71 (1994).
[4] D. D. Koelling, A. M. Boring, and J. H. Wood, Solid State Commun. **47**, 227 (1983).
[5] H. L. Tuller and A. S. Nowick, J. Phys. Chem. Solids **38**, 859 (1977).
[6] E. Wuilloud, B. Delley, W.-D. Schneider, and Y. Baer, Phys. Rev. Lett. **53**, 202 (1984).
[7] M. A. Panhans and R. N. Blumenthal, Solid State Ion. **60**, 279 (1993).
[8] C. Binet, A. Badri, and J.-C. Lavalley, J. Phys. Chem. **98**, 6392 (1994).
[9] J. Stubenrauch and J. M. Vohs, J. Catalysis **159**, 50 (1996).
[10] M. Romeo, K. Bak, J. El Fallah, F. le Normand, and L. Hilaire, Surf. Interface Anal. **20**, 508 (1993).
[11] J. Soria, A. Martinez-Arias, and J. Conesa, J. Chem. Soc. Faraday Trans. **91**, 1669 (1995).
[12] M. Matsumoto, K. Soda, K. Ichikawa, S. Tanaka, Y. Taguchi, K. Jouda, and O. Aita, Phys. Rev. B **50**, 11 340 (1994).
[13] J. C. Conesa, Surf. Sci. **339**, 337 (1995).
[14] T. X. T. Sayle, S. C. Parker, and C. R. A. Catlow, Surf. Sci. **316**, 329 (1994).
[15] J. W. Dawicke and R. N. Blumenthal, J. Electrochem. Soc. **133**, 904 (1986).
[16] I. K. Naik and T. Y. Tien, J. Phys. Chem. Solids **39**, 311 (1978).
[17] I. Riess, R. Koerner, M. Ricken, and J. Noelting, Solid State Ion. **28-30**, 539 (1988).
[18] P. W. Tasker, Surf. Sci. **87**, 315 (1979).
[19] J.-C. Parlebas, A. Kotani, and S. Tanaka, Prog. Theor. Phys. Suppl. **101**, 271 (1990).
[20] J. M. Honig and A. W. Czanderna, Phys. Chem. Solids **6**, 96 (1958).